Supplementary Information
PhysDock: A Physics-Guided All-Atom Diffusion Model for Protein-Ligand Complex Prediction

Kexin Zhang[1,4,+], Yuanyuan Ma[2,+], Jiale Yu[1,+], Huiting Luo[2], Jinyu Lin[2], Yifan Qin[1,6], Xiangcheng Li[2], Qian Jiang[5], Fang Bai[2], Jiayi Dou[2,*], Jie Zheng[1,*], Jingyi Yu[1,*], and Liping Sun[3,*]

[1]School of Information Science and Technology, ShanghaiTech University, Shanghai, 201210, China
[2]School of Life Science and Technology, ShanghaiTech University, Shanghai, 201210, China
[3]iHuman Institute, ShanghaiTech University, Shanghai, 201210, China
[4]Lingang Laboratory, Shanghai, 200031, China
[5]School of Computing, Australian National University, Canberra, 2601, Austrilia
[6]Cellverse Co., Ltd., Shanghai, 201210, China
[*]doujy@shanghaitech.edu.cn; zhengjie@shanghaitech.edu.cn; yujingyi@shanghaitech.edu.cn; sunlp@shanghaitech.edu.cn
[+]these authors contributed equally to this work

Contents

1 Additional data details

Featurization and data augmentation are described in the Methods section of the main text. The MSA featurization pipeline is adapted from AlphaFold2, while the MSA pairing scheme follows that of AlphaFold3. Additional details on data and feature processing are provided below.

1.1 Filtering

We extensively processed the Plinder dataset to construct the training and validation sets for PhysDock, as follows:

1. Removing systems with a resolution greater than 9 Å.
2. Removing systems containing RNA, DNA, and peptides.
3. Removing systems with ligands that have missing atoms.
4. Removing systems present in the benchmark dataset.
5. Removing systems with only a ligand or only a receptor.
6. Removing systems in the bio assembly where atoms, especially ligand atoms, have clashes (non-hydrogen atom distances less than 1 Å).

Ultimately, we obtained approximately 260,000 training and validation systems after filtering.

1.2 Metadata Processing

To accelerate dataset loading, we saved the following metadata:

1. `pdb_id_meta_data`: storing the structure determination method (*e.g.*, x-ray diffraction), release date, resolution, and all PDB chain IDs for each system.
2. `chain_id_meta_data`: storing the sequence of the specified chain_id, the sequence3 composed of CCD identifiers, and the MD5 code of the sequence. The MD5 code is used to retrieve existing MSA features and uniprot MSA features.
3. `ccd_id_meta_data`: storing all conformer features corresponding to each CCD conformer.
4. `train_val_sample_id_meta_data`: storing the sampling weight assigned to each training sample.

The weight for each sample is calculated based on the combined weight of the receptor and ligand. The receptor weight, ($W_{\text{receptor\_identity}}$), is determined by sequence identity, using a 40% sequence identity threshold. The ligand weight, ($W_{\text{ligand\_identity}}$) uses a 100% identity (*i.e.*, the weight is identical for ligands that are exactly the same).

$$W = W_{\text{receptor}} \times W_{\text{ligand}} = W_{\text{receptor\_identity}} \times W_{\text{ligand\_identity}}$$

The resulting weights are then used to guide the selection of the entire PDB structure for training, as well as to determine the receptor and ligand for sample localization. Additionally, they are used to process the model input for training according to the cropping strategy.

2 Model details

The network architecture and pseudocode (shown below) incorporate key innovations from AlphaFold2, AlphaFold3, Llama3, and Stable Diffusion 3, but is specifically tailored for molecular docking tasks.

2.1 Model Inputs

The input features of the model can be broadly categorized into sequence-related features, conformer-related features, backbone-related features, physical priors, and positional features. Below, we provide a brief description of each of these main feature categories.

Input Feature	Shape	Feature Type	Description
msa_feat	$[N_{msa}, N_{token}, 32]$	Sequence Feature	MSA-related features obtained from the processing of MSA and deletion matrix.
target_feat	$[N_{msa}, N_{token}, 32]$	Sequence Feature	Sequence-related features derived from the processing of the sequence and MSA profile.
ref_feat	$[N_{atom}, 32]$	Conformer Feature	Reference conformer node-related features generated for each residue or ligand by RDKit.
ref_pos	$[N_{atom}, 3]$	Conformer Feature	Randomly generated coordinated by RDKit.
ref_space_uid	$[N_{atom}]$	Conformer Feature	A unique ID of each conformer to distinguish atoms in different conformers.
rel_tok_feat	$[N_{token}, N_{token}, 32]$	Conformer Feature	Edge-related features for the reference conformer of ligand, zero for the receptor.
token_bonds	$[N_{msa}, N_{token}, 32]$	Conformer Feature	Covalent bonds for each atom in the reference conformer.
dgram_feat	$[N_{token}, N_{token}, 40]$	Backbone Feature	Distance Gram features computed for backbone $C\beta$ atoms.
key_res_feat	$[N_{token}, 7]$	Physical Priors	Indicators to mark whether a token is a key residue.
pocket_res_feat	$[N_{token}]$	Physical Priors	Indicators to mark whether a token is a pocket residue.
residue_index	$[N_{token}]$	Position Feature	Residue index in each chain.
asym_id	$[N_{token}]$	Position Feature	Unique chain IDs.
entity_id	$[N_{token}]$	Position Feature	Unique entity IDs.
sym_id	$[N_{token}]$	Position Feature	IDs to distinguish different chains of the same entity.

Table 1. Details of model input features.

2.2 Primitives

Below, we will present the primary network layers that constitute PhysDock. All attention mechanisms incorporate a gating mechanism, and some attention mechanisms introduce QK norm to stabilize the numerical values of the latent representations.

Algorithm 1 AdaLayerNormZero

def AdaLayerNormZero($\{x_i\}\{t\}$)

$t \leftarrow \text{silu}(t)$
$x_i \leftarrow \text{LayerNorm}(s, \text{affine} = \text{False})$
$shift \leftarrow \text{Linear}(t)$
$scale \leftarrow \text{Linear}(t)$
$gate \leftarrow \text{Linear}(t)$
$x_i \leftarrow x_i \odot (1 + scale) + shift$
return $\{x_i\}, \{gate\}$

Algorithm 2 FeedForward

def FeedForward($\{x_i\}$)

$x \leftarrow \text{silu}(\text{Linear}(x)) \odot \text{Linear}(x)$
$x \leftarrow \text{Linear}(x)$
return $\{x_i\}$

Algorithm 3 Transition

def Transition($\{x_i\}$)

$x_i \leftarrow \text{RMSNorm}(x_i)$
$x_i \leftarrow \text{FeedForward}(x_i)$
return $\{x_i\}$

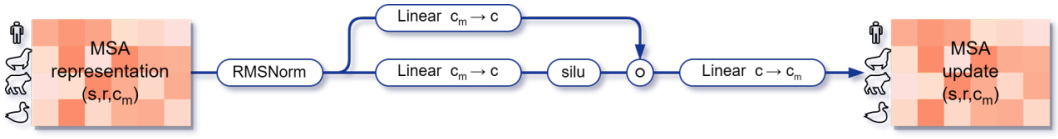

Figure 1. MSATransition layer.

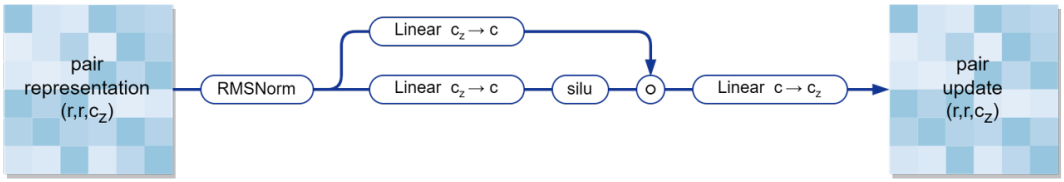

Figure 2. PairTransition layer.

Algorithm 4 DiTTransition

def DiTTransition($\{x_i\}, \{t\}$)

$x_i, g_i \leftarrow \text{AdaLayerNormZero}(x_i, t)$
$x_i \leftarrow \text{FeedForward}(x_i) \odot g_i$
return $\{x_i\}$

Algorithm 5 ScaledDotProductAttention

def SDPA($\{x_i\}\{b^h_{ij}\}$)

$q^h_i \leftarrow \text{Linear}(x)$
$k^h_i \leftarrow \text{Linear}(x)$
$v^h_i \leftarrow \text{Linear}(x)$
$a^h_{ij} \leftarrow \text{softmax}_j\left(\frac{1}{\sqrt{c}} {q^h_i}^\top k^h_j + b^h_{ij}\right)$
$x_i \leftarrow \sum_j a^h_{ij} c^h_j$
return $\{x_i\}$

Algorithm 6 ScaledDotProductAttentionNobias

def SDPANoBias($\{x_i\}$)

$q^h_i \leftarrow \text{Linear}(x)$
$k^h_i \leftarrow \text{Linear}(x)$
$v^h_i \leftarrow \text{Linear}(x)$
$a^h_{ij} \leftarrow \text{softmax}_j\left(\frac{1}{\sqrt{c}} {q^h_i}^\top k^h_j\right)$
$x_i \leftarrow \sum_j a^h_{ij} c^h_j$
return $\{x_i\}$

Algorithm 7 AttentionWithPairBias

def AttentionWithPairBias($\{x_i\}, \{t\}$)

$x_i \leftarrow \text{RMSNorm}(x_i)$
$b^h_{ij} \leftarrow \text{RMSNorm}(z_{ij})$
$g_i \leftarrow \text{Linear}(x_i)$
$x_i \leftarrow \text{SDPA}(x_i, z^h_{ij}) \odot g_i$
return $\{x_i\}$

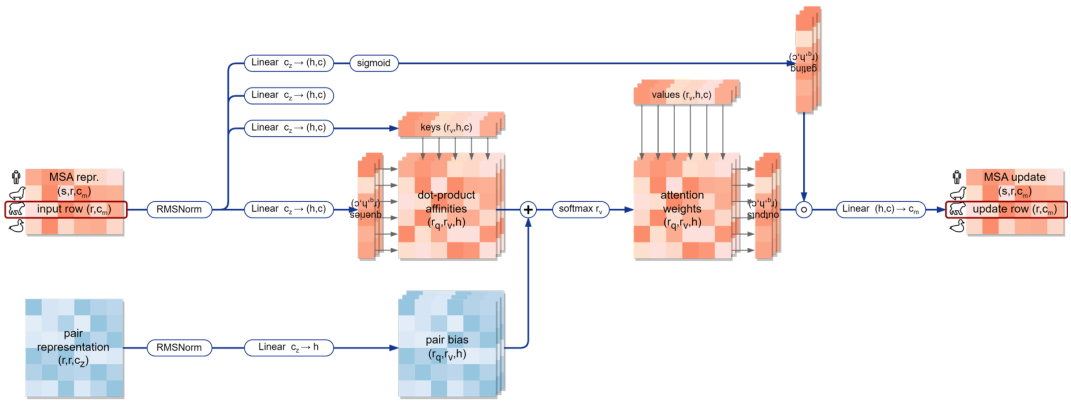

Figure 3. MSARowAttentionWithPairBias.

Algorithm 8 MSAColumnAttention

def MSAColumnAttention($\{m_{si}\}$)

$m_{si} \leftarrow \text{RMSNorm}(m_{si})$
$m_{si} \leftarrow \text{SPDANobias}(m_{si}{}^{\top})^{\top}$
return $\{m_{si}\}$

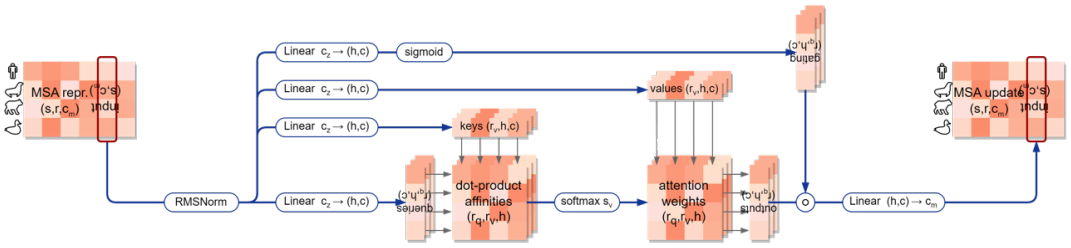

Figure 4. MSA Column attention.

Algorithm 9 TriangleAttention

def TriangleAttention($\{z_{ij}\}$, transpose = False)

if transpose **then**
  $z_{ij} \leftarrow z_{ji}$
end if
$z_{ij} \leftarrow \text{RMSNorm}(z_{ij})$
$b^h_{ij} \leftarrow \text{Linear}(z_{ij})$
$g_{ij} \leftarrow \text{Linear}(z_{ij})$
$z_{ij} \leftarrow \text{SDPA}(z_{ij}, b^h_{ij})$
$z_i j \leftarrow z_{ij} \odot g_{ij}$
if transpose **then**
  $z_{ij} \leftarrow z_{ji}$
end if
return $\{z_{ij}\}$

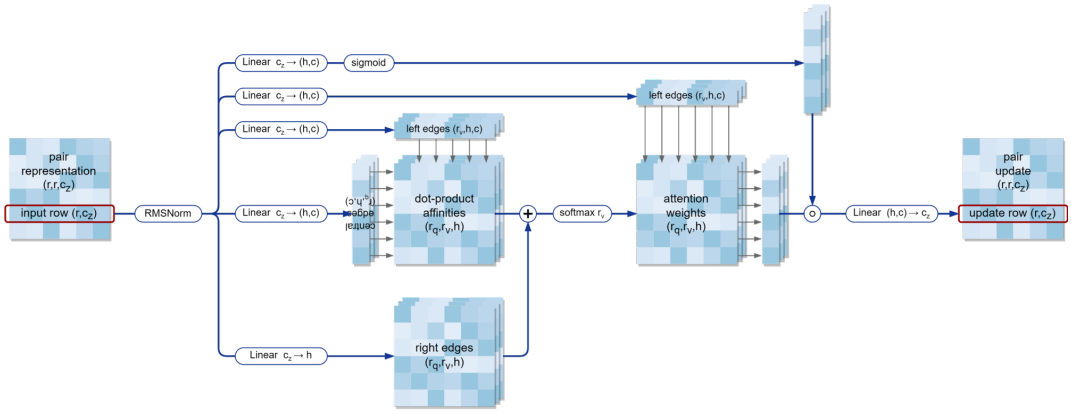

Figure 5. TriangleAttention layer.

Algorithm 10 DiTAttention

def DiTAttention($\{x_i\}, \{z_{ij}\}, \{t\}$)

$x_i, g_i \leftarrow \text{AdaLayerNormZero}(x_i, t)$
$b^h_{ij} \leftarrow \text{Linear}(\text{LayerNorm}(z_{ij}))$
$x_i \leftarrow \text{SDPA}(x_i, b^h_{ij})$
$x_i \leftarrow x_j \odot g_i$
return $\{x_i\}$

Algorithm 11 TriangleUpdate

def TriangleUpdate($\{z_{ij}\}$, transpose = False)

if transpose **then**
  $z_{ij} \leftarrow z_{ji}$
end if
$z_{ij} \leftarrow \text{RMSNorm}(z_{ij})$
$q_{ij} \leftarrow \text{Linear}(z_{ij}) \odot \text{sigmoid}(\text{Linear}(z_{ij}))$
$k_{ij} \leftarrow \text{Linear}(z_{ij}) \odot \text{sigmoid}(\text{Linear}(z_{ij}))$
$g_{ij} \leftarrow \text{sigmoid}(\text{Linear}(z_{ij}))$
$z_{iI} \leftarrow \sum_j z_{ij} z_{Ij}$
$z_{ij} \leftarrow \text{Linear}(\text{RMSNorm}(z_{ij})) \odot g_{ij}$
if transpose **then**
  $z_{ij} \leftarrow z_{ji}$
end if
return $\{z_{ij}\}$

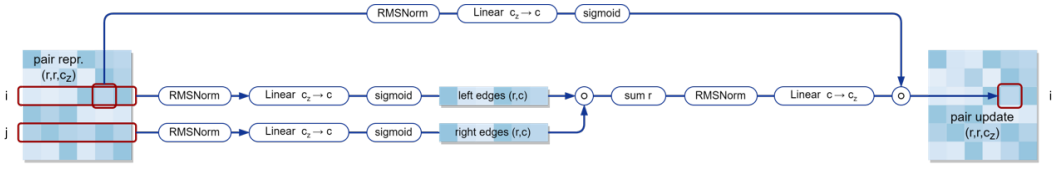

Figure 6. TriangleUpdate layer.

Algorithm 12 OuterProductMean

def OuterProductMean($\{m_{si}\}$)

$m_{si} \leftarrow \text{RMSNorm}(m_{si})$
$q_{si} \leftarrow \text{Linear}(m_{si})$
$k_{si} \leftarrow \text{Linear}(m_{si})$
$z_{ij} \leftarrow \sum_s q_{si} k_{sj}$
$z_{ij} \leftarrow \text{RMSNorm}(z_{ij})$
return $\{z_{ij}\}$

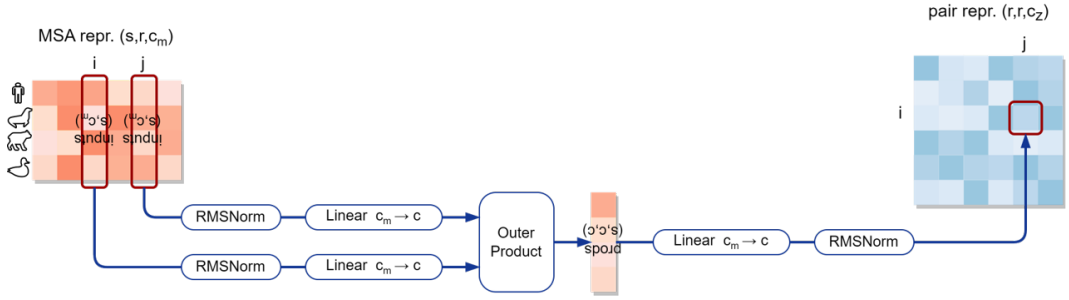

Figure 7. OuterpRroductMean layer. Instead of directly calculating the mean, normalization is employed in the final step.

Algorithm 13 Timesteps

def Timesteps($\{t\}, num\_channels, flip\_sin\_to\_cos, downscale\_freq\_shift, scale$)

$half\_dim \leftarrow num\_channels // 2$
$exponent \leftarrow -\log(\text{max\_period}) \cdot \text{arange}(0, half\_dim) / (half\_dim - downscale\_freq\_shift)$
$emb\_base \leftarrow \exp(exponent)$
$emb \leftarrow t[:, \text{None}] \cdot emb\_base[\text{None}, :]$
$emb \leftarrow scale \cdot emb$
$emb \leftarrow \text{concat}(\sin(emb), \cos(emb), \text{dim} = -1)$
if flip_sin_to_cos **then**
    $emb \leftarrow \text{concat}(emb[:, half\_dim:], emb[:, : half\_dim], \text{dim} = -1)$
end if
if num_channels % 2 == 1 **then**
    $emb \leftarrow \text{pad}(emb, (0, 1, 0, 0))$
end if
return $\{emb\}$

Algorithm 14 TimestepEmbeddings

def TimestepEmbeddings($\{t\}$)

$timesteps\_proj \leftarrow \text{Timesteps}(t)$
$conditioning \leftarrow \text{Linear}(\text{SiLU}(timesteps\_proj))$
return $\{conditioning\}$

2.3 Layers

Below, we will illustrate the connection methods of all the key network layers.

Algorithm 15 AtomTransformer

def AtomTransformer($\{s_i\}, \{z_{ij}\}, N_{\text{blocks}}$)

for all $l \in [1, ..., N_{\text{blocks}}]$ **do**
  s_i += AttentionWithPairBias(s_i, z_{ij})
  s_i += Transition(s_i)
end for
return $\{s_i\}$

Algorithm 16 RelPosEmbedder

def RelPosEmbedder({asym_id}, {sym_id}, {entity_id}, {residue_index}, {rel_tok_feat})

s_max ← 2 # Window of chain index
r_max ← 32 # Window of residue index
chain_same ← (asym_id[..., None] == asym_id[..., None, :])
entity_same ← (entity_id[..., None] == entity_id[..., None, :])
residue_offset ← residue_index[..., None] − residue_index[..., None, :] + r_max
clipped_residue_offset ← clamp(residue_offset, $min = 0, max = 2 \cdot$ r_max)
d_res ← where(chain_same, clipped_residue_offset, $2 \cdot$ r_max + 1)
rel_pos_feat ← one_hot(d_res, arange($0, 2 \cdot$ r_max + 2))
chain_offset ← sym_id[..., None] − sym_id[..., None, :] + s_max
clipped_chain_offset ← clamp(chain_offset, $0, 2 \cdot$ s_max)
d_chain ← where(or(chain_same, not(entity_same)), $2 \cdot$ s_max + 1, clipped_chain_offset)
rel_chain_feat ← one_hot(d_chain, arange($0, 2 \cdot$ s_max + 2))
rel_feat ← concat(rel_pos_feat, rel_tok_feat, entity_same[..., None], rel_chain_feat)
return Linear(rel_feat)

Algorithm 17 EvolutionTransformer

def EvolutionTransformer($\{m_{si}\}, \{z_{ij}\}, N_{\text{blocks}}$)

for all $l \in [1, ..., N_{\text{blocks}}]$ **do**
  m_{si} += AttentionWithPairBias(m_{si}, z_{ij})
  m_{si} += MSAColumnAttention(m_{si})
  m_{si} += Trainsition(m_{si})
  z_{ij} += OuterProductMean(m_{si})
  z_{ij} += TriangleUpdate(z_{ij}, transpose = False)
  z_{ij} += TriangleUpdate(z_{ij}, transpose = True)
  z_{ij} += TriangleAttention(z_{ij}, transpose = False)
  z_{ij} += TriangleAttention(z_{ij}, transpose = True)
  z_{ij} += Trainsition(z_{ij})
end for
return $\{m_{si}\}\{z_{ij}\}$

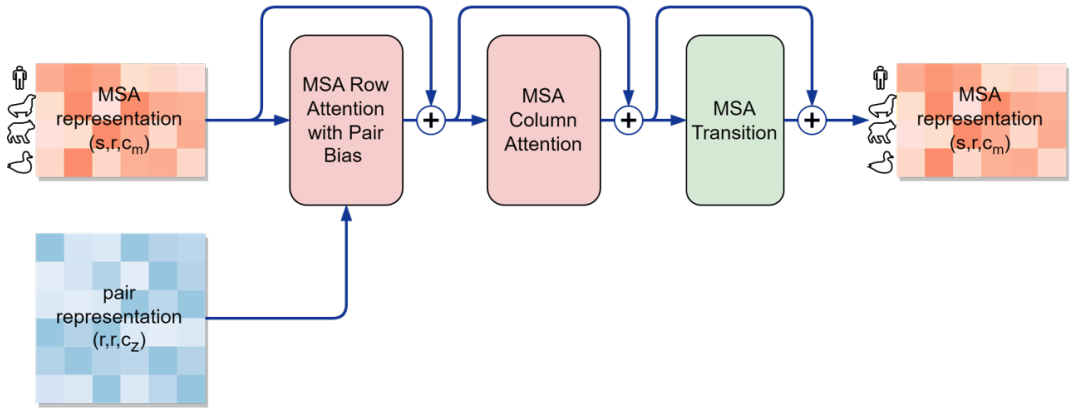

Figure 8. MSABlock inside EvolutionTransformerBlock.

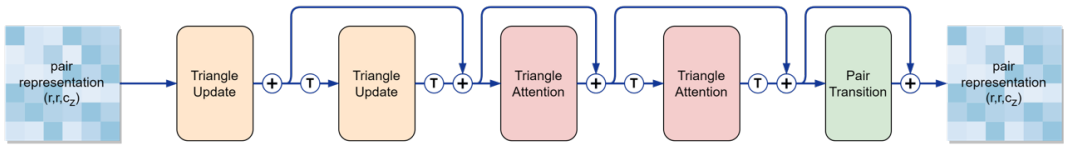

Figure 9. TriangleTransformerBlock.

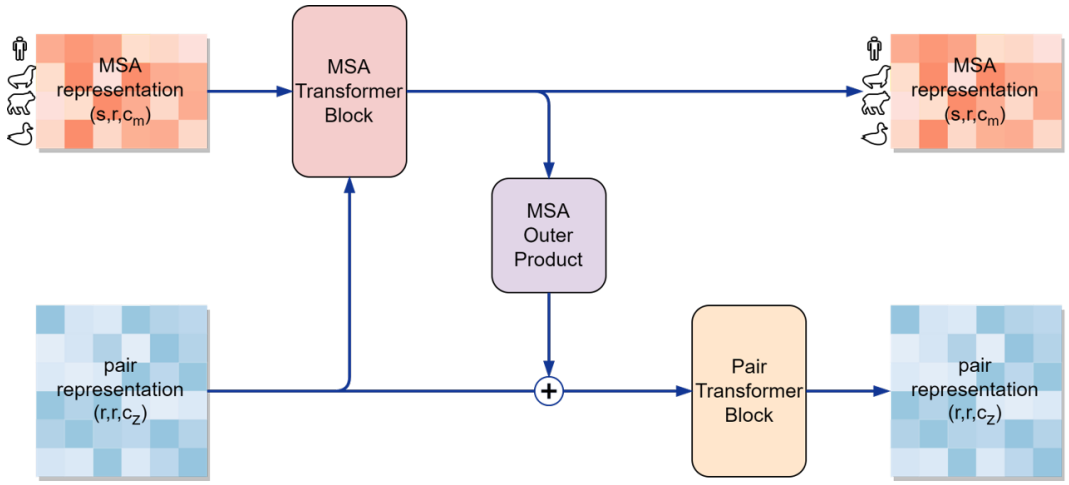

Figure 10. Evolution Transformer Block.

Algorithm 18 TriangleTransformer

def TriangleTransformer($\{z_{ij}\}, N_{\text{blocks}}$)

for all $l \in [1, ..., N_{\text{blocks}}]$ **do**
  z_{ij} += TriangleUpdate(z_{ij}, transpose = False)
  z_{ij} += TriangleUpdate(z_{ij}, transpose = True)
  z_{ij} += TriangleAttention(z_{ij}, transpose = False)
  z_{ij} += TriangleAttention(z_{ij}, transpose = True)
  z_{ij} += Trainsition(z_{ij})
end for
return $\{z_{ij}\}$

Algorithm 19 PairTransformer

def PairTransformer($\{s_i\}, \{z_{ij}\}, N_{\text{blocks}}$)

for all $l \in [1, ..., N_{\text{blocks}}]$ **do**
  z_{ij} += TriangleUpdate(z_{ij}, transpose = False)
  z_{ij} += TriangleUpdate(z_{ij}, transpose = True)
  z_{ij} += TriangleAttention(z_{ij}, transpose = False)
  z_{ij} += TriangleAttention(z_{ij}, transpose = True)
  z_{ij} += Trainsition(z_{ij})
  s_i += AttentionWithPairBias(s_i, z_{ij})
  s_i += Transition(s_i)
end for
return $\{s_i\}\{z_{ij}\}$

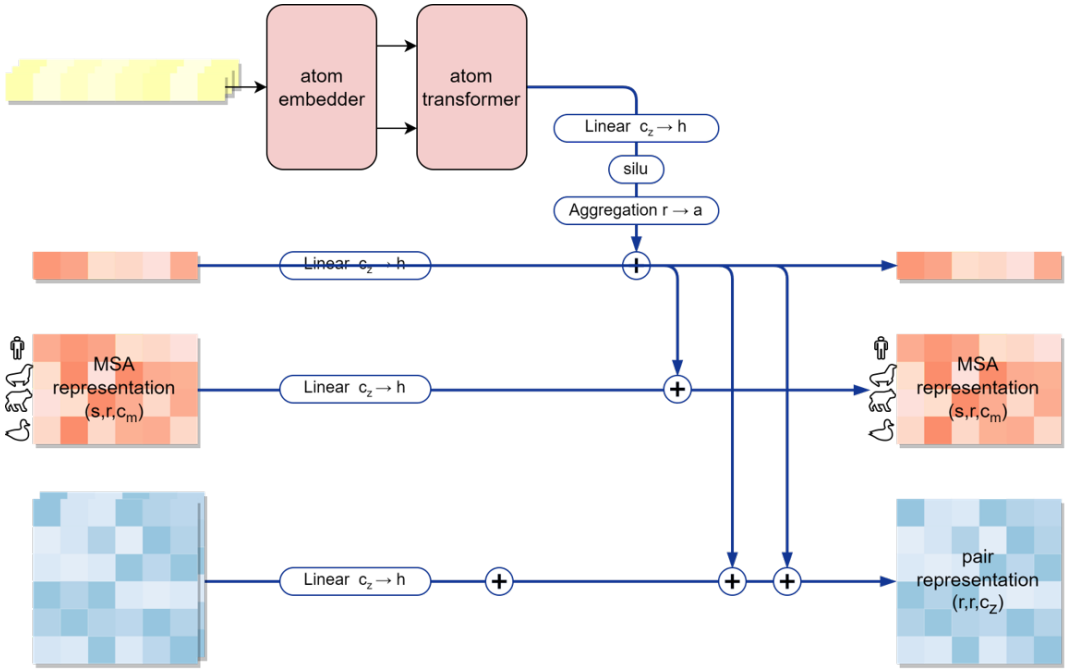

Figure 11. Update Atomwise representations after PairTransformer.

Algorithm 20 DiffusionTransformer

def DiffusionTransformer($\{s_i\}, \{z_{ij}\}, \{t\}, N_{\text{blocks}}$)

for all $l \in [1, ..., N_{\text{blocks}}]$ **do**
  s_i += DiTAttention(s_i, z_{ij}, t)
  s_i += DitTransition(s_i, t)
end for
return $\{s_i\}$

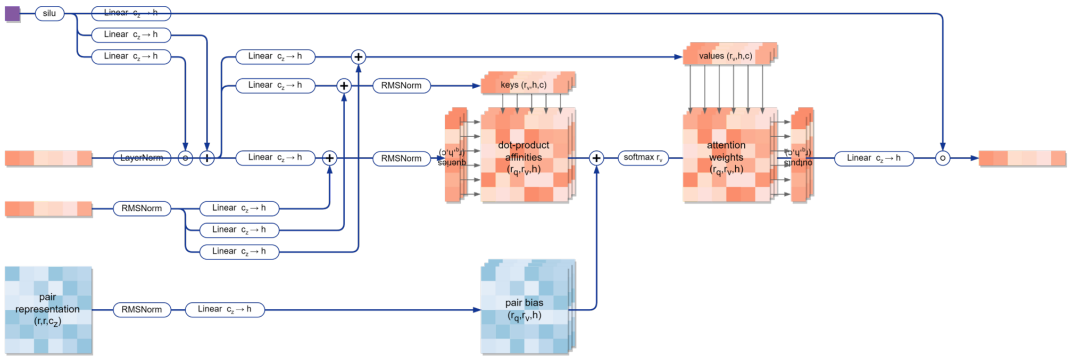

Figure 12. Tokenwise Diffusion Transformer Attention.

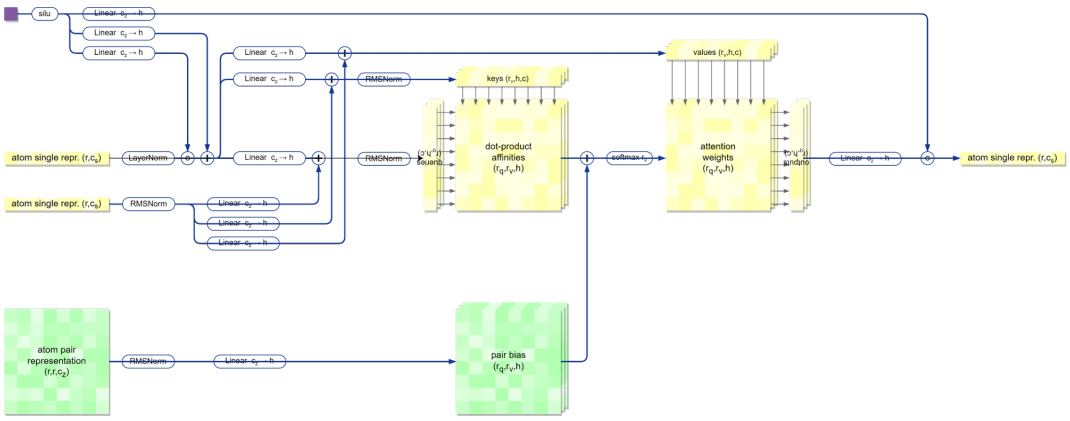

Figure 13. Atomwise Diffusion Transformer Attention.

Algorithm 21 TemplatePairEmbedder

def TemplatePairEmbedder($\{z\}$, dgram_feat)

1: $z \leftarrow \text{Linear}(\text{RMSNorm}(z)) + \text{Linear}(\text{dgram\_feat})$
2: $z \leftarrow \text{TriangleTransformer}(z)$
3: $z \leftarrow \text{Linear}(\text{ReLU}(\text{RMSNorm}(z)))$
4: **return** $\{z\}$

3 Loss

Our model employs only the diffusion loss as the final loss function $\mathscr{L}_{\text{loss}}$, which integrates the Mean Squared Error (MSE) and the smooth LDDT loss:

$$\mathscr{L}_{\text{loss}} = \alpha_{\text{diffusion}} \cdot (\hat{t}^2 + \sigma_{\text{data}}^2)/(\hat{t} \cdot \sigma_{\text{data}})^2 \cdot \mathscr{L}_{\text{MSE}} + \alpha_{\text{diffusion}} \cdot \mathscr{L}_{\text{smooth\_lddt}}$$

where $\alpha_{\text{diffusion}}$ is a constant equals 4.0, σ_{data} is a constant equals 16.0.

4 Training details

Training was conducted in two phases with a maximum crop size of 384: an initial 50,000 steps using bfloat16 (bf16) mixed precision with a batch size of 48, followed by 200,000 steps using full-precision (fp32) training with the same batch size.

5 Baseline details

In this study, baseline predictions were generated using existing docking methods, each producing 40 binding modes. For classical docking tools, AutoDock Vina v1.2.3 was executed with an exhaustiveness of 32, a ligand binding site threshold of $20 \sim 25$Å a protein–ligand threshold of 4Å a docking box size of 25Å$\times$ 25Å $\times$ 25Å and a grid spacing of 1ÅGlide was performed as follows: (i) protein structures were optimized using the Protein Preparation in the Maestro module of Schrödinger (v2022-3), including hydrogen addition, bond order assignment, completion of missing side chains and loops, removal of water molecules located more than 5 Å away from the ligand, optimization of the hydrogen-bond network, and energy minimization using the OPLS-2005 force field until the heavy-atom RMSD converged to 0.3 Å ; (ii) ligand preparation was carried out using LigPrep, ultilizing the Epik module to generate possible protonation and ionization states at a target pH of 7.0 ± 2.0; (iii) conformers were generated, and the one with the lowest energy—based on the OPLS-2005 force field—was selected as the input for subsequent docking experiments; (iv) receptor grids were constructed using the Receptor Grid Generation module in Schrödinger, with an inner box (centered on the co-crystallized ligand) of 10 Å $\times$ 10 Å $\times$ 10 Å and an outer box extending 10Å in all directions beyond the inner box; and (v) ligand–protein docking was performed using the Glide module in standard precision (SP) mode.

For semi-flexible DL models, SurfDock first identifies amino acid residues within an 8Å radius of the target ligand to define the binding surface, computes physical features (including molecular surface, charge, hydrophobicity, and curvature), and generates a PLY file for subsequent sampling. Interformer produces an initial UFF-optimized ligand conformer, and independently defines the docking pocket as residues within a 10Å distance from the target ligand. Uni-Mol Docking V2 (Uni-Mol version 1.0.0) takes both the ligand and the full complex structure as input, selects a region within a 10Å radius of the target ligand to define the docking center and grid size, and utilizes the UFF-optimized ligand from Interformer.

For flexible DL models, NeuralPLexer operates with default settings—batched structure sampling (40 samples, 40 steps, block size 10) combined with Langevin simulated annealing. AlphaFold v3.0.0 was processed with seed 42 to generate 40 structures per complex and Chai-1 v0.5.2 was used in the MSA input mode without ESM representations. Both flexible DL models use protein sequence and ligand SMILES notation to predict the protein–ligand complex. All experiments were performed under a uniform setup, with every method executed using its default parameters to ensure consistency.

6 Supplementary Figures

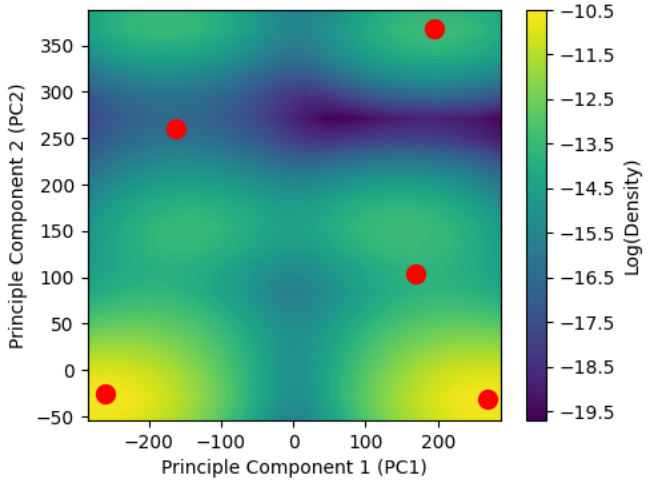

Figure 14. Log-density visualization of 1,000 AlphaFold3-generated samples (PDB ID: 7AA0, seeds 41 and 42). The x- and y-axes represent the first and second principal components of the RMSD distance matrix, respectively. Red points denote the Top-5 ranked samples.

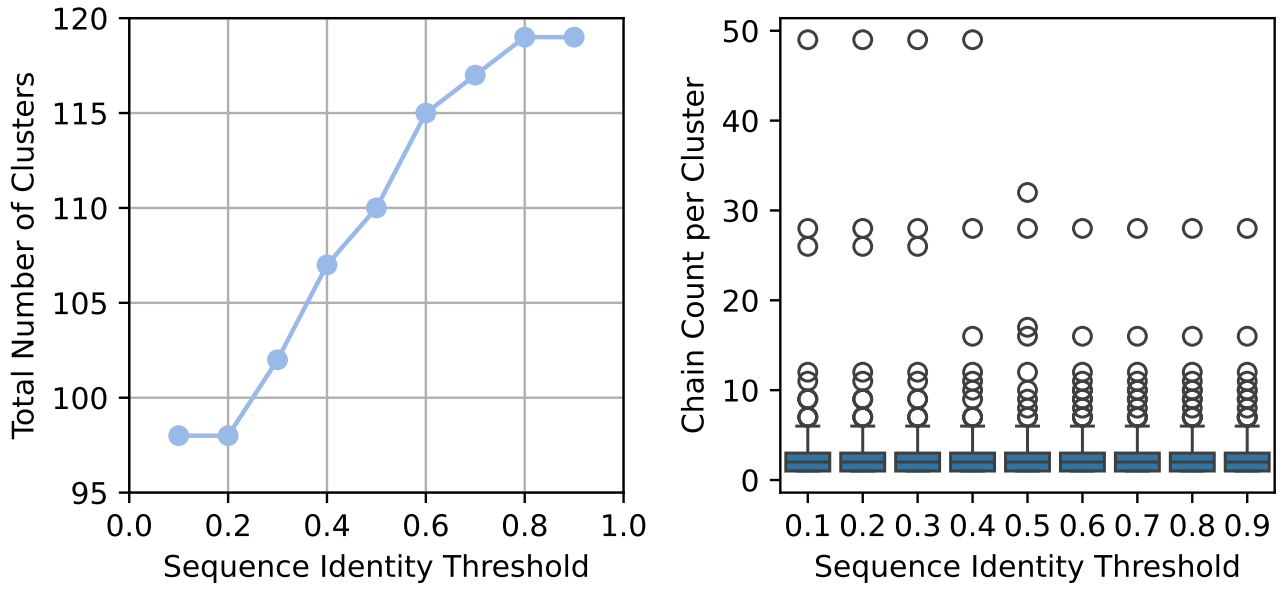

Figure 15. Analysis of the PhiBench dataset using MMseqs2 clustering at various sequence identity thresholds. The left panel illustrates the variation in the total number of clusters as the sequence identity threshold increases from 0.1 to 0.9. The right panel presents a detailed distribution of the number of protein chains per cluster.

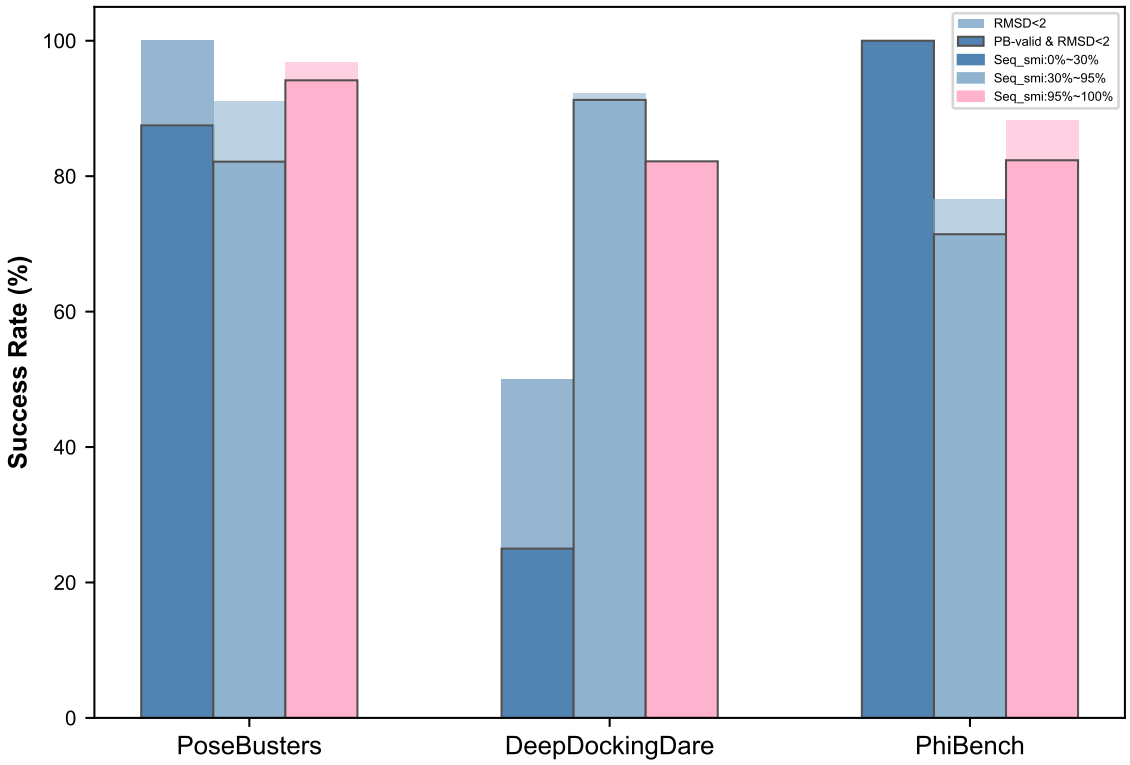

Figure 16. Performance of PhysDock on three datasets, categorized by sequence similarity to the Plinder training set (PoseBusters: 428 samples, subsets: 8/ 112/ 308 for low/ medium/ high similarity; DeepDockingDare: 356 samples, subsets: 4/ 206/ 146; PhiBench: 206 samples, subsets: 6/ 98/ 102). Docking success rates are computed under two criteria: PAL-RMSD $\leq$ 2.0 Å, and PB-valid & PAL-RMSD $\leq$ 2.0 Å.

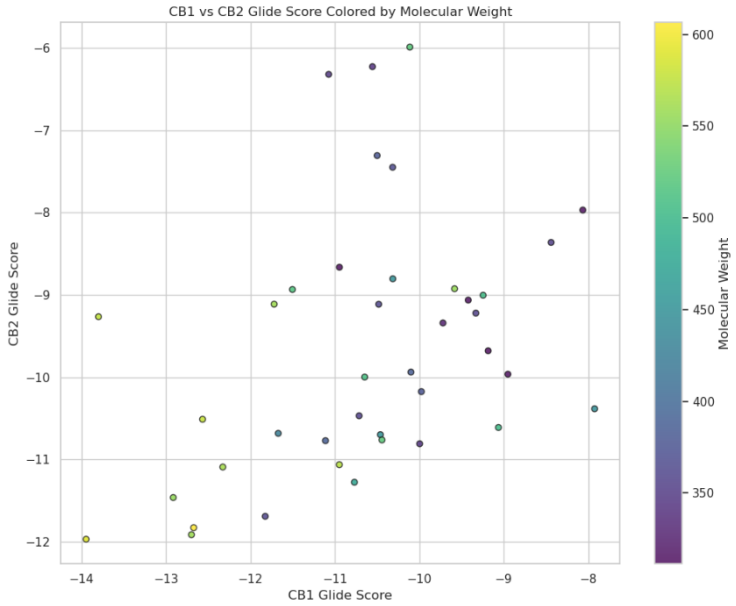

Figure 17. Glide scores for 40 compounds docked to CB1 and CB2 receptors using PhysDock. Each point represents a ligand, color-coded by molecular weight.

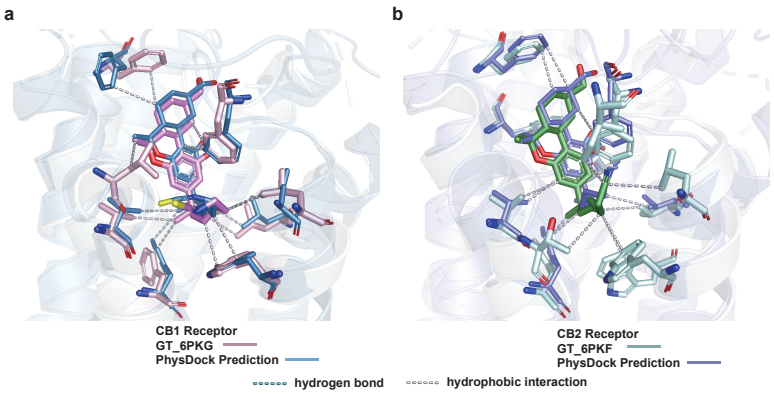

Figure 18. The combined pattern graph predicted by Physdock and the overlapping graph of Ground Truth.

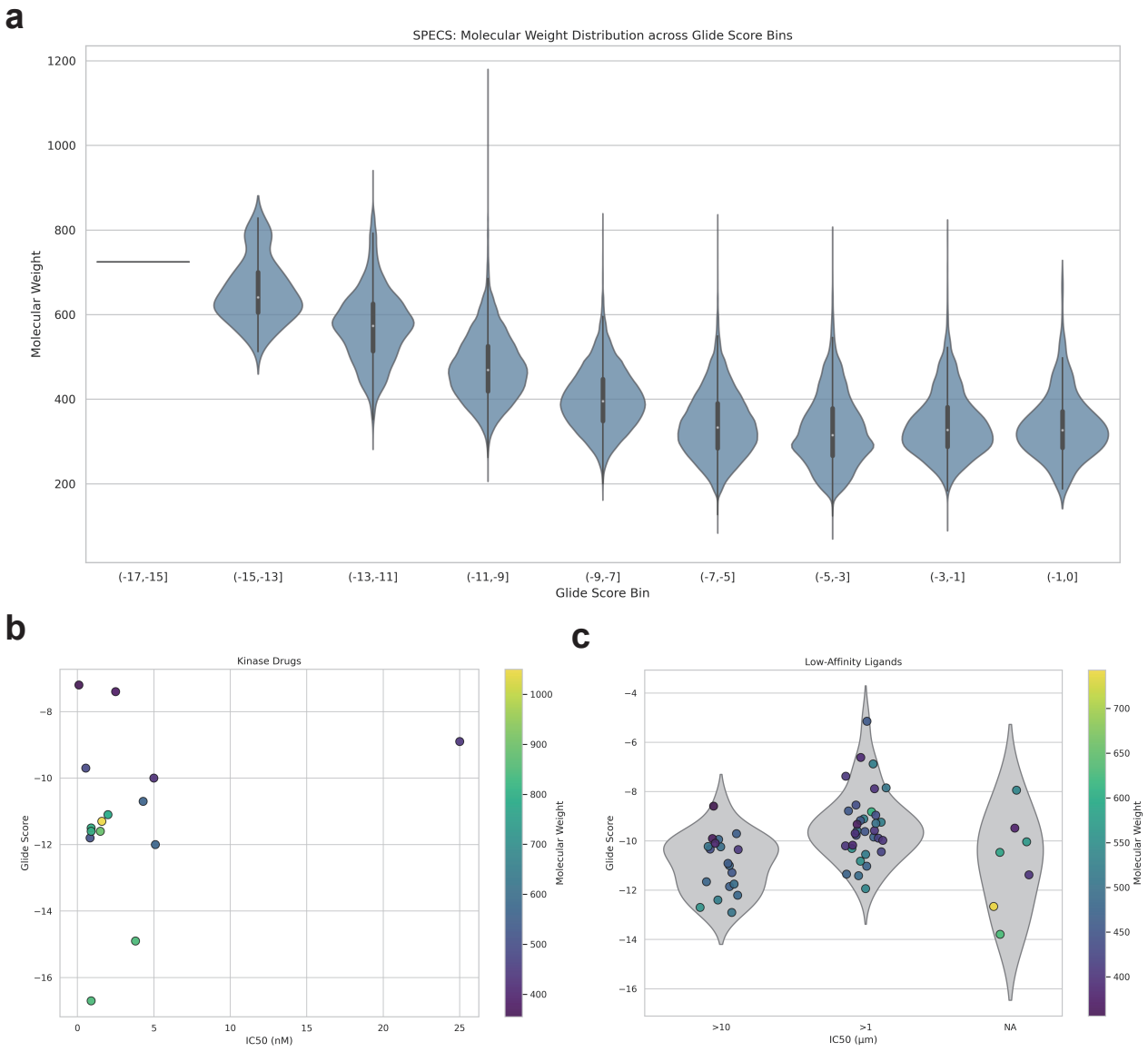

Figure 19. **(a)** Violin plot showing the distribution of molecular weights for SPECS compounds across different Glide score bins from PhysDock screening against the NTRK3 kinase. **(b)** Glide scores of known drug candidates docked to the NTRK3 kinase using PhysDock plotted against their IC_{50} values, with points color-coded by molecular weight. **(c)** Glide scores of low-affinity ligands docked to the NTRK3 kinase using PhysDock grouped by IC_{50} categories, with points color-coded by molecular weight.

7 Supplementary Tables

Table 2. Docking success rates of existing methods with prior binding pocket information across three benchmark datasets.

Method	PoseBusters		DeepDockingDare		PhiBench	
	PAL-RMSD	**PB-valid**	**PAL-RMSD**	**PB-valid**	**PAL-RMSD**	**PB-valid**
PhysDock	408/428	389/428	317/356	309/356	171/206	160/206
SurfDock	347/428	337/428	291/355	242/355	132/184	131/184
Interformer	332/428	300/428	251/356	229/356	123/180	114/180
AlphaFold3	299/426	297/426	212/356	202/356	105/206	98/206
Uni-Mol Docking V2	257/428	209/428	142/356	135/356	98/184	96/184
Chai-1	267/428	264/428	140/356	127/356	92/206	87/206
DiffDock-L	232/428	150/428	81/344	68/344	74/186	66/186
Glide	228/428	199/428	142/356	120/356	47/185	45/185
Vina	179/428	172/428	122/355	119/355	47/198	45/198
DiffDock	186/427	104/427	75/344	66/344	57/186	48/186
DynamicBind	188/420	185/420	82/334	81/334	100/184	98/184
NeuralPLexer	84/419	57/419	15/333	11/333	37/186	31/186

Table 3. Interaction recovery rates and ground-truth interaction counts across three benchmark datasets.

PoseBusters

Model	hydrogen bonds	hydrophobic interactions	salt bridges	pi-stacking	pi-cation interactions
PhysDock*	72.2	75.6	87.6	64.0	43.1
Uni-Mol Docking V2*	66.8	56.4	79.9	68.2	66.7
SurfDock*	64.7	60.3	80.4	50.6	55.0
Glide*	51.0	56.2	75.8	44.3	26.9
DiffDock-l*	54.9	43.8	67.7	50.7	32.5
DynamicBind	56.2	52.3	76.4	38.7	21.2
Interformer*	46.1	45.0	56.5	53.6	0.0
Vina*	39.7	41.0	49.3	40.9	19.5
DiffDock*	41.8	37.1	52.2	36.7	22.5
AlphaFold3	48.2	37.6	17.6	11.5	10.4
Chai-1	44.9	26.1	17.7	8.0	6.9
NeuralPLexer	16.6	14.0	20.7	11.4	8.5

Interaction counts — Hydrogen bonds: 1688, Hydrophobic interactions: 1323, Salt bridges: 369, Pi-stacking: 170, Pi-cation interactions: 52

DeepDockingDare

Model	hydrogen bonds	hydrophobic interactions	salt bridges	pi-stacking	pi-cation interactions
Uni-Mol Docking V2*	56.3	52.1	83.2	54.5	62.9
SurfDock*	56.9	56.3	78.4	38.8	46.3
PhysDock*	43.0	59.3	38.7	44.9	23.5
Interformer*	34.5	40.8	48.5	42.1	41.7
Vina*	30.3	36.7	48.0	42.4	38.8
Glide*	33.7	39.5	33.7	37.8	14.3
DiffDock-l*	30.7	25.6	48.9	23.2	26.6
DiffDock*	25.8	23.7	47.7	23.3	26.5
DynamicBind	30.3	22.9	53.2	17.1	14.8
AlphaFold3	30.8	24.0	31.5	32.1	13.6
Chai-1	27.7	15.4	22.4	10.7	7.8
NeuralPLexer	9.4	12.4	9.3	16.2	1.1

Interaction counts — Hydrogen bonds: 893, Hydrophobic interactions: 1548, Salt bridges: 97, Pi-stacking: 41, Pi-cation interactions: 23

PhiBench

Model	hydrogen bonds	hydrophobic interactions	salt bridges	pi-stacking	pi-cation interactions
Uni-Mol Docking V2*	63.4	49.0	85.9	63.4	50.8
SurfDock*	57.2	48.7	82.7	35.1	38.0
PhysDock*	52.6	53.5	51.9	58.2	17.8
DiffDock-l*	53.4	37.6	73.6	34.9	29.5
Glide*	43.0	42.7	79.2	31.8	17.4
Interformer*	37.8	36.0	51.1	43.6	28.2
DynamicBind	47.5	36.8	57.4	29.6	14.9
DiffDock*	39.7	32.5	62.4	26.2	17.6
Vina*	34.7	31.6	60.1	21.7	24.2
Chai-1	46.3	18.9	20.2	11.5	6.8
NeuralPLexer	27.1	16.7	30.6	9.0	12.9
AlphaFold3	45.2	30.0	14.1	0.0	5.0

Interaction counts — Hydrogen bonds: 1002, Hydrophobic interactions: 583, Salt bridges: 164, Pi-stacking: 33, Pi-cation interactions: 38

Table 4. Experimental binding free energies and Glide scores for all compounds docked to CB1 and CB2 receptors using PhysDock.

Name	Molecules	CB1_ΔG_exp (kcal/mol)	CB1_PhysDock Glide (kcal/mol)	CB2_ΔG_exp (kcal/mol)	CB2_PhysDock Glide (kcal/mol)
MK-0364 [2]	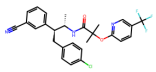	-13.49	-11.501	-9.23	-8.935
ACEA [1]	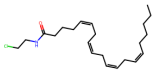	-12.15	-10.315	-7.82	-7.45
AM-11542 [2]	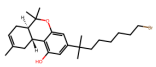	-12.12	-10.46	-13.59	-10.699
ACPA [1]	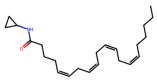	-11.88	-10.554	-8.44	-6.228
THC [2]	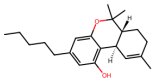	-11.65	-9.42	-10.08	-9.064
SR-147778 [2]	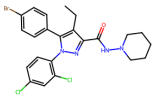	-11.53	-10.111	-8.73	-5.99
AM-251 [2]	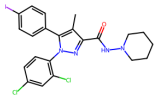	-11.08	-9.582	-7.69	-8.926
WIN-55,212-2 [2]	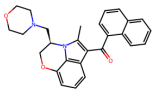	-10.96	-11.669	-11.84	-10.683
R-methanandamide [1]	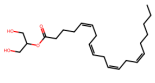	-10.57	-10.48	-8.36	-9.114
2-AG [1]	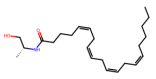	-9.93	-10.498	-9.39	-7.308

Name	Molecules	CB1_ΔG_exp (kcal/mol)	CB1_PhysDock Glide (kcal/mol)	CB2_ΔG_exp (kcal/mol)	CB2_PhysDock Glide (kcal/mol)
anandamide [1]	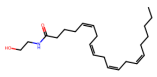	-9.9	-11.072	-7.84	-6.321
PNR-4-20 [1]	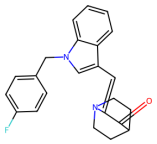	-9.33	-11.823	-12	-11.691
UR-144 [2]	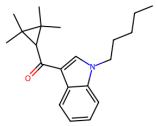	-9.3	-10.945	-11.93	-8.665
SR-144528 [2]	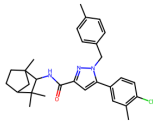	-8.73	-10.767	-12.58	-11.277
VJ-115 [1]	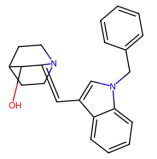	-7.52	-9.995	-8.6	-10.809
CBD [2]	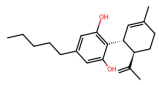	-7.24	-8.063	-7.334	-7.97
AM-630 [2]	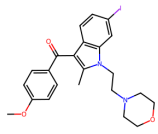	-7.2	-9.244	-10.23	-9.005
GW842166X [3]	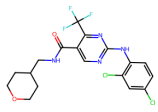	>-6.17	-10.313	-9.96	-8.805
JWH-151 [3]	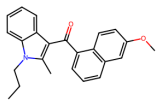	>-6.82	-10.712	-10.26	-10.469
L-759,633 [4]	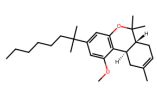	-6.55	-10.098	-10.5	-9.939

Name	Molecules	CB1_ΔG_exp (kcal/mol)	CB1_PhysDock Glide (kcal/mol)	CB2_ΔG_exp (kcal/mol)	CB2_PhysDock Glide (kcal/mol)
GW-405,833 [5]	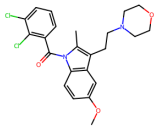	-7.26	-7.924	-11.49	-10.384
PF-03550096 [5]	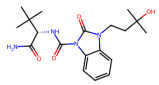	-11.05	-9.975	-7.96	-10.176
APD371 [5]	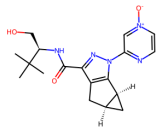	>-6.82	-9.33	-11.2	-9.222
Cannabilactone [5]	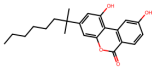	-8.73	-8.439	-12.4	-8.363
HU-211 [5]	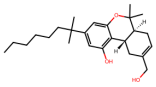	-7.78	-11.11	>-6.82	-10.772
7 [6]	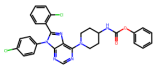	-11.72	-11.718	-6.78	-9.113
9 [6]	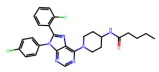	-10.52	-10.441	-8.16	-10.763
10 [6]	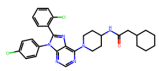	-11.89	-12.325	-7.68	-11.092
18 [6]	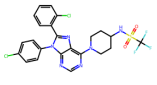	-11.21	-10.946	-7.29	-11.063
Otenabant [7]	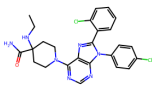	-12.49	-10.646	-6.98	-9.999

Name	Molecules	CB1_ΔG_exp (kcal/mol)	CB1_PhysDock Glide (kcal/mol)	CB2_ΔG_exp (kcal/mol)	CB2_PhysDock Glide (kcal/mol)
12 [7]	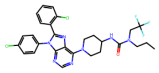	-12.22	-12.67	-7.58	-11.8287
15 [7]	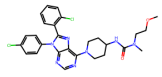	-13.08	-12.912	-7.69	-11.463
25 [7]	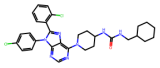	-12.34	-12.565	-6.98	-10.512
29 [7]	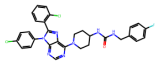	-11.63	-13.944	>-6.82	-11.969
30 [7]	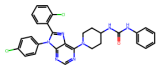	-11.12	-12.697	>-6.82	-11.914
32 [7]	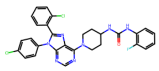	-11.46	-13.797	>-6.82	-9.266
AM1241 [8]	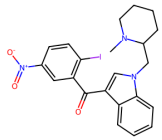	-7.23	-9.062	-10.67	-10.612
24 [9]	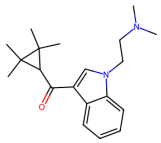	>-6.82	-9.184	-11.9	-9.68
36 [9]	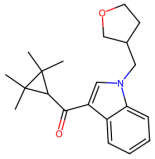	-8.46	-9.719	-13.44	-9.342
50 [9]	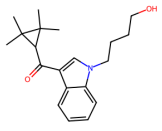	>-7.16	-8.95	-11.81	-9.964

Table 5. Docking results of kinase inhibitors across different models

Name	Molecules	Stage	IC50 (nM)	PhysDock_Glide (kcal/mol)
Repotrectinib	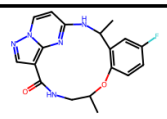	Approved	0.1	-7.2
Entrectinib	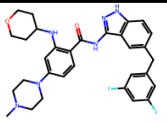	Approved	4.3	-10.7
Larotrectinib	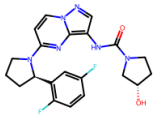	Approved	5-11	-10.0
Lestaurtinib	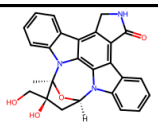	Phase III	25	-8.9
Selitrectinib		Phase I	2.5	-7.4
CH7057288	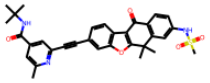	Preclinical	5.1	-12.0
Altiratinib	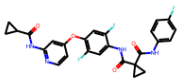	Preclinical	0.83	-11.8
CPD-085	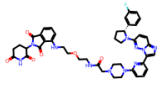	Preclinical	3.8	-14.9
Compound 30f	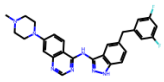	Preclinical	0.55	-9.7
CPD-141	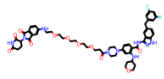	Preclinical	1.6	-11.3
CPD-145	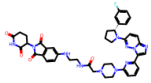	Preclinical	0.9	-11.5
CPD-053	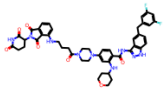	Preclinical	1.5	-11.6
CPD-211	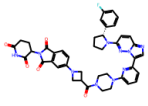	Preclinical	2	-11.1
CPD-143	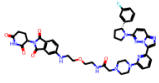	No progress	0.9	-16.7
CPD-159	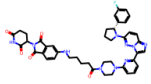	No progress	0.9	-11.6

Table 6. Experimental IC_{50} values and Glide scores for known drug candidates and weak binders docked to NTRK3 kinase using PhysDock.

Name	Molecules	IC50 (μM)	PhysDock_Glide (kcal/mol)
B30 [10]	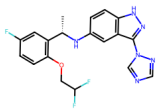	NA	-11.4
7n [11]	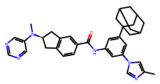	>10	-12.7
7m [11]	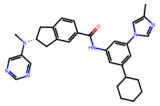	>10	-12.9
7l [11]	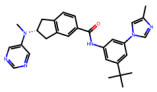	>10	-12.2
7k [11]	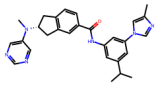	>10	-11.9
7j [11]	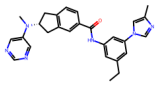	>10	-11.3
7i [11]	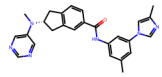	>10	-10.3
7h [11]	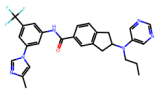	>10	-12.4
7g [11]	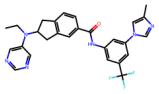	>10	-10.2
7f [11]	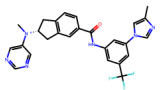	>10	-11.8

Name	Molecules	IC50 (μM)	PhysDock_Glide (kcal/mol)
7e [11]	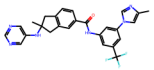	>10	-10.2
7d [11]	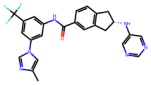	>10	-11.0
7c [11]	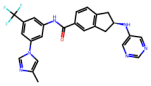	>10	-11.7
7b [11]	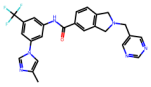	>10	-9.9
7a [11]	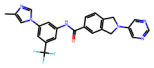	>10	-9.7
6n [12]	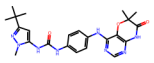	>10	-10.9
6k [12]	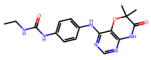	>10	-8.6
6j [12]	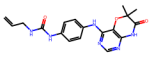	>10	-9.9
6i [12]	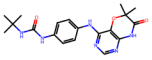	>10	-10.1
6g [12]	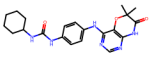	>10	-10.4

Name	Molecules	IC50 (μM)	PhysDock_Glide (kcal/mol)
32h [13]	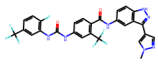	>1	-8.8
32e [13]	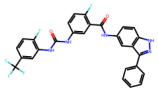	>1	-10.8
32c [13]	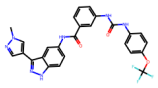	>1	-11.9
32b [13]	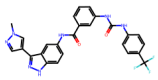	>1	-6.9
32a [13]	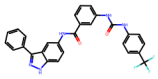	>1	-10.5
26k [13]	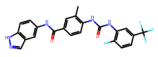	>1	-9.8
26h [13]	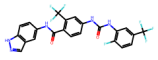	>1	-9.1
26g [13]	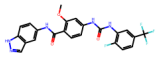	>1	-11.4
26c [13]	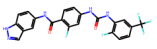	>1	-11.4
26a [13]	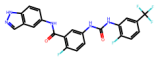	>1	-11.0

Name	Molecules	IC50 (μM)	PhysDock_Glide (kcal/mol)
23c [13]	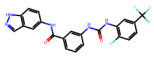	>1	-10.4
23b [13]	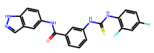	>1	-9.2
23a [13]	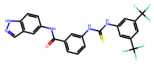	>1	-5.1
21b [13]	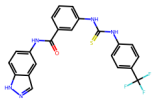	>1	-8.5
21a [13]	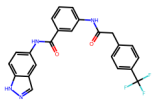	>1	-9.8
19c [13]	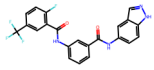	>1	-10.3
19b [13]	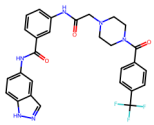	>1	-9.6
16z [13]	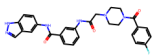	>1	-9.0
16y [13]	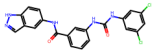	>1	-7.8
16w [13]	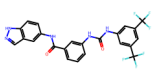	>1	-8.8

Name	Molecules	IC50 (μM)	PhysDock_Glide (kcal/mol)
16v [13]	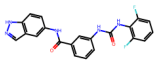	>1	-7.4
16t [13]	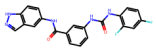	>1	-9.6
16s [13]	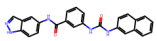	>1	-9.9
16o [13]	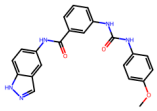	>1	-9.7
16m [13]	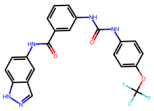	>1	-9.2
16i [13]	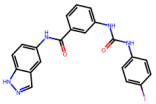	>1	-9.3
16h [13]	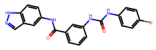	>1	-9.6
16g [13]	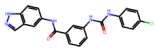	>1	-10.0
16f [13]	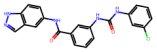	>1	-10.2
16d [13]	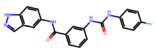	>1	-10.2

Name	Molecules	IC50 (μM)	PhysDock_Glide (kcal/mol)
16c [13]	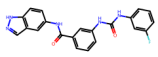	>1	-6.6
16aa [13]	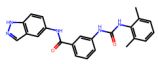	>1	-7.9
16a [13]	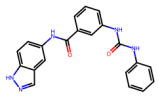	>1	-9.3
22 [14]	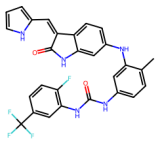	NA	-7.9
19 [14]	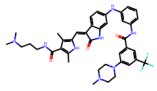	NA	-12.7
16 [14]	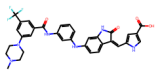	NA	-13.8
7 [14]	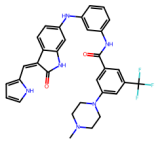	NA	-10.5
5_1 [15]	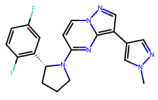	NA	-9.5
5_2 [14]	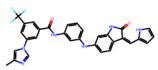	NA	-10.0

References

1. Yang, J. F. *et al.* Binding modes and selectivity of cannabinoid 1 (cb1) and cannabinoid 2 (cb2) receptor ligands. *ACS chemical neuroscience* **11**, 3455–3463 (2020).
2. Ji, B. *et al.* Prediction of the binding affinities and selectivity for cb1 and cb2 ligands using homology modeling, molecular docking, molecular dynamics simulations, and mm-pbsa binding free energy calculations. *ACS chemical neuroscience* **11**, 1139–1158 (2020).
3. Markt, P., Feldmann, C. & Rollinger, J. M. Discovery of novel cb2 receptor ligands by a pharmacophore-based virtual screening workflow. *J. medicinal chemistry* **52**, 369–378 (2009).
4. Gareau, Y. *et al.* Structure activity relationships of tetrahydrocannabinol analogues on human cannabinoid receptors. *Bioorganic Medicinal Chem. Lett.* **6**, 189–194 (1996).
5. Han, S., Thatte, J., Buzard, D. J. & Jones, R. M. Therapeutic utility of cannabinoid receptor type 2 (cb(2)) selective agonists. *J. medicinal chemistry* **56**, 8224–8256 (2013).
6. Fulp, A., Bortoff, K. & Zhang, Y. Peripherally selective diphenyl purine antagonist of the cb1 receptor. *J. medicinal chemistry* **56**, 8066–8072 (2013).
7. Amato, G., Manke, A. & Wiethe, R. Functionalized 6-(piperidin-1-yl)-8,9-diphenyl purines as peripherally restricted inverse agonists of the cb1 receptor. *J. medicinal chemistry* **62**, 6330–6345 (2019).
8. Bingham, B. *et al.* Species-specific in vitro pharmacological effects of the cannabinoid receptor 2 (cb2) selective ligand am1241 and its resolved enantiomers. *Br. journal pharmacology* **151**, 1061–1070 (2007).
9. Frost, J. M. *et al.* Indol-3-ylcycloalkyl ketones: effects of n1 substituted indole side chain variations on cb(2) cannabinoid receptor activity. *J. medicinal chemistry* **53**, 295–315 (2010).
10. Qin, Q. *et al.* Discovery of novel indazole derivatives as second-generation trk inhibitors. *Eur. J. Medicinal Chem.* **276**, 116640 (2024).
11. Zhu, D. *et al.* 2-amino-2,3-dihydro-1h-indene-5-carboxamide-based discoidin domain receptor 1 (ddr1) inhibitors: Design, synthesis, and in vivo antipancreatic cancer efficacy. *J. medicinal chemistry* **62**, 7431–7444 (2019).
12. Pan, S. *et al.* Structural optimization and structure-activity relationship studies of 6,6-dimethyl-4-(phenylamino)-6h-pyrimido[5,4-b][1,4]oxazin-7(8h)-one derivatives as a new class of potent inhibitors of pan-trk and their drug-resistant mutants. *J. medicinal chemistry* **65**, 2035–2058 (2022).
13. Wang, G. *et al.* Rational design and crystallographic analysis of novel isoform-selective trka inhibitors for cancer therapy. *Acta pharmaceutica Sinica* **13**, 440–443 (2023).
14. Albaugh, P. *et al.* Discovery of gnf-5837, a selective trk inhibitor with efficacy in rodent cancer tumor models. *ACS medicinal chemistry letters* **3**, 140–145 (2012).
15. Zhuo, L. S. *et al.* Discovery of next-generation tropomyosin receptor kinase inhibitors for combating multiple resistance associated with protein mutation. *ACS medicinal chemistry letters* **64**, 15503–15514 (2021).